Q. J. R. Meteorol. Soc. (1999), **125**, pp. 993–1016

Observations of oblate hail using dual polarization radar and implications for hail-detection schemes

By T. J. SMYTH*, T. M. BLACKMAN and A. J. ILLINGWORTH
University of Reading, UK

(Received 4 September 1997; revised 6 July 1998)

SUMMARY

Coincidental radar measurements and *in situ* ground-truth observations of large, oblate hail has allowed new insights into the fall mode of oblate hailstones. The effect of the fall mode upon hail-detection algorithms using multi-parameter radar is investigated and discussed, as is the vexed problem of extracting realistic rainfall rates in regions where hail and rain coexist. Observations presented here show that oblate hail can be associated with non-zero values of differential reflectivity, Z_{DR}, which, together with the coincidental values of the linear depolarization ratio, suggest some degree of alignment. Although large hail can dominate backscatter through the diameter-to-the-sixth-power dependence, even if it is aligned it makes a negligible contribution to specific differential phase, K_{DP}. Rainfall rates extracted using K_{DP} in the presence of hail are more robust than those using the contaminated reflectivity in the horizontal polarization, Z_H, and Z_{DR} measurements, but proposed hail-detection algorithms which compare the observed values of K_{DP} and Z_H do seem error prone. The hailstones measured in this study were of sufficient dimensions to allow Mie scattering to occur at S-band (wavelength $\lambda = 9.75$ cm). This served to complicate the interpretation of the differential-phase measurements. A new hail-detection algorithm has been formulated which compares the differential phase predicted from Z_H and Z_{DR} with that actually observed. This avoids the problem of estimating K_{DP} from the derivative of a noisy differential-phase profile.

KEYWORDS: Differential-phase shift Differential reflectivity Multiparameter radar Precipitation rate

1. INTRODUCTION

The differentiation between rain and hail has been a long-standing objective of radar meteorologists. Various methods with differing degrees of sophistication have been suggested. The first attempts used reflectivity only measurements. Mason (1971) suggested a 55 dBZ reflectivity threshold as an indicator of the presence of hail. Waldvogel *et al.* (1979) describe a method involving the maximum reflectivity, the height of the 45 dBZ level above the 0 °C isotherm and the vertical reflectivity profile. An automatic hail-detection algorithm is currently being advocated for use on the US Next-Generation Weather Doppler Radar (NEXRAD; Kessinger *et al.* 1995), which is based upon an examination of the echo intensity and its evolution within the storm. Essentially it involves recognizing an echo greater than 55 dBZ in the mid-level of the cloud. The procedure is complex, and no information is provided about the location and extent of the hail fall. This is the greatest problem for all hail-detection techniques which rely solely upon reflectivity. The presence of hail can only be inferred in a gross sense, large hail giving a larger value of reflectivity, Z, than rain due to the D^6 weighting, where D is drop diameter; differences in the refractive index of ice and liquid water introduce further uncertainty. Another operational algorithm has been formulated by Hardaker and Auer (1994) which combines satellite infrared (I.R.) cloud-top temperature and radar reflectivity to delineate between hail and rain.

Lemon (1995) postulated the use of a Mie-scattering artifact, called a 'three body scatter spike', for operationally forecasting large hail. This is a weaker echo radially aligned behind a highly reflective (>63 dBZ) echo core. It is found almost exclusively aloft, has low reflectivity (<20 dBZ) and is relatively short (<8 km). Zrnić (1987) examined the radar artifact and explained that this radar echo feature is the result of a triple reflection from the hail shaft; Mie scattering at S-band would occur for particles larger than about 7 mm.

* Corresponding author, present address: Plymouth Marine Laboratory, Prospect Place, Plymouth PL1 3DH, UK. e-mail: T.J.Smyth@pml.ac.uk

Another approach to hail detection has made use of dual-wavelength radar (e.g. Atlas and Ludlam 1961) where Mie scattering by large hail leads to reduced reflectivity at the shorter wavelength. Dual-wavelength studies are plagued with the difficulty of distinguishing between reduced Z due to Mie scattering and attenuation effects at the shorter wavelength, and the very different backscatter from wet and dry hail.

Dual-polarization methods that distinguish rain from hail assume that hailstones, even if oblate, tumble as they fall and appear isotropic to the radar. Bringi *et al.* (1984), using a dual-polarization technique, found that in regions of hail the differential reflectivity, Z_{DR}, rapidly drops to values near 0 dB, but exhibits larger positive values in the surrounding rain. The reflectivity either increases or maintains a relatively high value in the hail. Using distrometer measurements Aydin *et al.* (1986) simulated values of backscattered reflectivity in the horizontal polarization, Z_H and Z_{DR}. They found that the raindrop size distributions fell within a well-defined region of Z_H–Z_{DR} space. From these distrometer results an empirically derived hail signal (H_{DR}) algorithm was formulated as a measure of the departure of the observed Z_H from the hail–rain boundary. The algorithm took the following form:

$$H_{DR} = Z_H - f(Z_{DR}), \tag{1}$$

$$f(Z_{DR}) = \begin{cases} 27, & Z_{DR} \leqslant 0 \text{ (dB)} \\ 19Z_{DR} + 27, & 0 \leqslant Z_{DR} \leqslant 1.74 \text{ (dB)} \\ 60, & Z_{DR} > 1.74 \text{ (dB)}. \end{cases}$$

Positive values of H_{DR} should indicate hail, but the derivation of the precise position of the hail demarcation line on a Z_H/Z_{DR} plot is not clear.

The algorithm also implies that the hail medium is isotropic; but the very fact that hailstones are often oblate suggests that they cannot always tumble randomly. In these cases there must be a degree of anisotropy in the falling-hailstone population. Recent studies into the detection of hail within rain–hail mixtures have made use of specific differential phase (e.g. Aydin *et al.* 1995); these are discussed in the next section.

In this paper we report in detail on coincidental multi-parameter radar and *in situ* measurements of a summer hailstorm which occurred in southern England on 10 July 1995.

2. Theory of polarization-radar parameters

Four radar parameters were used in this study to detect the hail: Z_H, Z_{DR}, linear depolarization ratio, LDR, and the differential-phase shift, ϕ_{DP}.

(*a*) *Measured polarization parameters*

Differential reflectivity is defined as (Seliga and Bringi 1976):

$$Z_{DR} = 10 \log_{10} \frac{Z_H}{Z_V} \text{ (dB)}, \tag{2}$$

where Z_V is the backscattered reflectivity in the vertical polarization. Z_{DR} is a measure of the reflectivity-weighted oblateness (Jameson 1983). Raindrops are oblate to a degree which increases with size, and fall with their minor axes oriented vertically; consequently

high positive values of Z_{DR} are associated with large oblate raindrops. Regions containing ice particles are usually characterized by lower values of Z_{DR}, despite any asphericity, because of their lower refractive index and tendency to tumble. The Aydin *et al.* (1986) hail-detection algorithm relies on hail being isotropic and having lower values of Z_{DR} than would be the case with rain.

The polarization parameter LDR can be used to distinguish between different hydrometeors. It is defined as:

$$LDR = 10 \log_{10} \frac{Z_{VH}}{Z_H} \text{ (dB)}, \tag{3}$$

where Z_H is the normal copolar return measured with horizontal polarization, and Z_{VH} is the cross-polar return measured in the horizontal for a vertically polarized transmitted signal. LDR senses oblate-particle fall mode; values of LDR above the Chilbolton radar (51.145°N, 1.437°W) antenna limit of −32 dB occur for particles which cant or tumble as they fall. In essence, only hydrometeors that have axes of symmetry that are canted with respect to the incident polarization will depolarize; because water has a higher dielectric constant than dry ice, the differences in the induced dipoles along the axes of the oblate wet particles are much larger, and so such wet particles have much higher values of LDR.

ϕ_{DP} is the difference in phase between the copolar radar returns measured with vertical and horizontal polarization ($\phi_V - \phi_H$); it is made up of three contributions: the range-integrated specific differential phase (K_{DP}), differential-phase shift on backscatter (δ) and a hardware offset (ϕ_0) which should be constant.

$$\phi_{DP}(r) = \phi_0 + \delta(r) + \int_0^r K_{DP}(r)\, dr \quad (^\circ), \tag{4}$$

where r is the range.

K_{DP} is the two-way specific differential phase. As the incident wave propagates through a region of oblate raindrops the horizontally polarized wave lags progressively behind the vertical one, hence ($\phi_V - \phi_H$) continually increases and its gradient, K_{DP}, is positive.

Sachidananda and Zrnić (1987) proposed that the two-way K_{DP} (° km^{-1}) at S-band is related to the rainfall rate (R; mm hr^{-1}) by:

$$K_{DP} = 0.0308\, R^{1.15}, \tag{5}$$

based on the drop shapes of Green (1975) and an exponential raindrop size spectrum of the form:

$$N(D) = N_0 \exp(-3.67 D/D_0) \quad (\text{m}^{-3}\text{mm}^{-1}), \tag{6}$$

where the intercept of the curve on the N axis, $N_0 = 8000$ m^{-3}mm^{-1}, D is the diameter and D_0 is the equivolumetric or median diameter. Both K_{DP} and R scale linearly with N_0 but because of the low power of the exponent in (5) the relationship between K_{DP} and R should be relatively insensitive to changes in N_0.

We shall use the relationship derived by Blackman and Illingworth (1994):

$$K_{DP} = 0.012\, R^{1.37} \quad (^\circ\text{km}^{-1}) \tag{7}$$

for $N_0 = 8000$ m^{-3}mm^{-1} based on slightly different drop-shapes, where the axial ratio, r_a, is related to the diameter D in mm, given by:

$$r_a = 1.075 - 0.065D - 0.0036D^2 + 0.0004D^3 \tag{8}$$

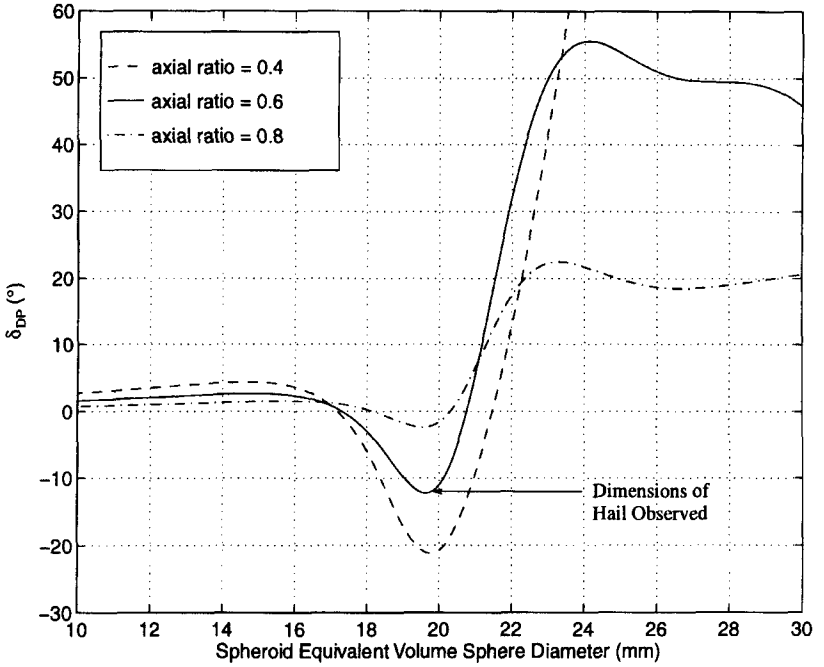

Figure 1. Differential-phase shift on backscatter δ_{DP} as a function of diameter for spongy hail (dielectric constant $\epsilon_r = 16.85 + 3.47i$) at S-band ($\lambda = 9.75$ cm) and temperature 0 °C. See text for further details.

for drops above 1.1 mm size; and the axial ratio is unity for drops smaller than 1.1 mm as proposed by Goddard *et al.* (1995) from the radar–distrometer comparisons of Goddard *et al.* (1982), subsequently supported by the theoretical work of Beard and Chuang (1987). In this case, for these 'new' drop shapes, because the exponent in (7) is 1.37 the relationship between K_{DP} and R is much more sensitive to changes in N_0 in the drop size spectrum.

At S-band δ is usually considered to be very small as it only occurs in the Mie regime, that is for raindrops or hailstones larger than 7 mm; it is only measurable if the hydrometeors have a preferred orientation (McCormick *et al.* 1979), not if randomly oriented. In this paper we confirm the results of Zrnić *et al.* (1993) that the neglect of δ is not a valid assumption, even at S-band, for large, wet, oblate hailstones that have an aligned fall mode. It is important to note that δ, being a backscatter effect, is a transitory change in ϕ_{DP} superposed on the general propagation effect, and can introduce ambiguity in the interpretation of the signal. The ϕ_0 contribution from the hardware is constant and can be subtracted.

(*b*) *Simple models of the differential-phase shift on backscatter*

Figure 1 shows the variation of δ with increasing diameter for spongy hail (30% water) at axial ratios of 0.4, 0.6 and 0.8 aligned with a vertical minor axis, calculated using T-matrix code (Waterman 1965). The scattering computations were carried out using a refractive index of a water and ice mixture calculated by the Bruggemann rule (O'Brien and Geodecke 1988). For 20 mm diameter spongy hail with an axial ratio between 0.4 and 0.6, δ is between $-10°$ and $-20°$, but δ can be as large as $+50°$ for a 25 mm diameter hailstone. Dry ice with dielectric constant ($\epsilon_r = 3.18 + 0.02i$ at 9.75 cm and 0 °C; Liebe *et al.* 1989), smaller than that of liquid water ($\epsilon_r = 79.30 + 25.70i$), gives much lower values of δ in the size range 0 to 35 mm in diameter. The values of δ for water as a function

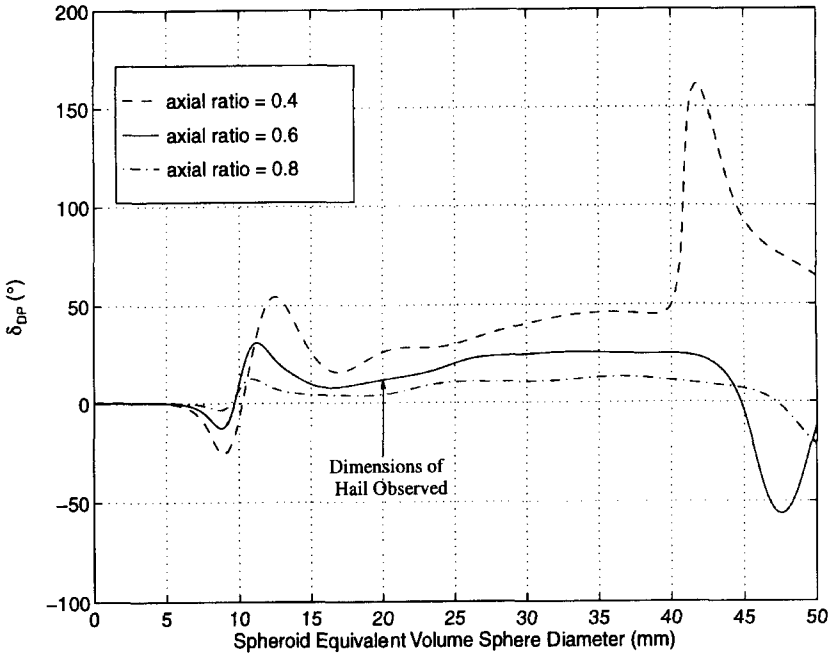

Figure 2. As Fig. 1 but for water ($\epsilon_r = 79.3 + 25.7i$).

of diameter and axial ratio are shown in Fig. 2. (For dry ice δ is a monotonic function of size reaching $+7°$ for a 25 mm diameter hailstone with an axial ratio of 0.6.) Equation 8 indicates that 8 mm raindrops have an axial ratio of 0.52, and so would, if monodispersed, produce δ of about $-10°$.

(*c*) K_{DP} *of hail*

In an anisotropic medium, such as rain, where the hydrometeors are oblate spheroids with their minor axes oriented in the vertical, ϕ_{DP} increases with range. If hail is assumed to be isotropic then it does not contribute to ϕ_{DP}. Figure 3 shows the variation of K_{DP} with increasing diameter for wet hailstones, axial ratio = 0.6, present in concentrations of 1 m^{-3}, with their major axes *aligned* in the horizontal; negative values arise because of Mie scattering. A single 10 mm hailstone per m^{-3} would give a Z of 60 dBZ, whereas 21.5 mm size would yield 80 dBZ. Cheng and English (1983) in an observational study, empirically derived a gamma size distribution for hailstone concentration. They showed that large hailstones are typically present in smaller concentrations than small hailstones. For example, they found that a 20 mm diameter hailstone has a maximum concentration of 6×10^{-3} m^{-3} whereas a 10 mm hailstone has a concentration an order of magnitude larger. Large hailstones tend to dominate the reflectivity ($\propto D^6$); taking the example of the monodispersed 20 mm hailstone, concentration $N = 6 \times 10^{-3}$ m^{-3}, results in $Z_H = 56$ dBZ and a K_{DP} of only 0.06° km^{-1}. In short, large hailstones give large values of reflectivity but negligible values of K_{DP}. This implies that lower values of K_{DP} coincidental with high values of reflectivity indicate an increased probability that the precipitation contains hail (Balakrishnan and Zrnić 1990). Balakrishnan and Zrnić showed that it was possible to distinguish the mixed-phase precipitation from either pure rain or pure hail by using Z_H and K_{DP}, and to infer the thermodynamic phase and orientation from Z_H and Z_{DR}.

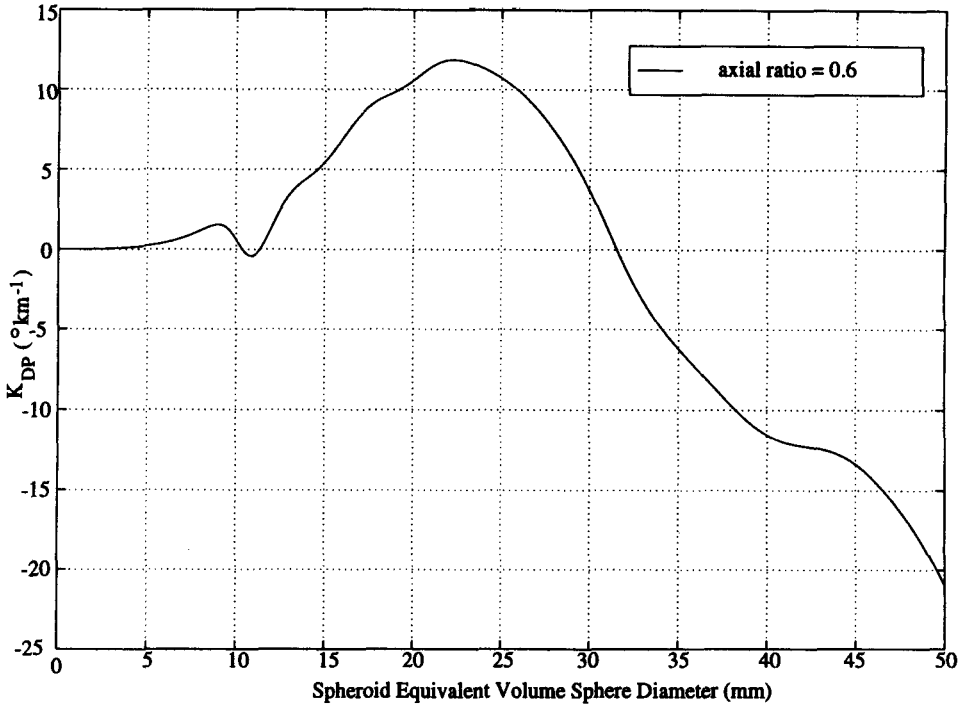

Figure 3. Range-integrated specific differential phase K_{DP} as a function of diameter for a wet hailstone (ϵ_r = 79.3 + 25.7i) of axial ratio = 0.6, concentration 1 m^{-3}.

They derived a relationship between K_{DP} (two way) and Z_H in pure rain from (5):

$$Z\ (\text{dBZ}) = 44 + 13.86 \log(K_{DP}) \tag{9}$$

by assuming an exponential raindrop size spectrum (see (6)) with $N_0 = 8000$ m^{-3}mm^{-1}. Two observational studies, consistent with theory, allowed them to conclude that K_{DP} yielded a good estimate of rain liquid water in a rain–hail mixture (they asserted that pure dry hail, as it is nearly isotropic with a small refractive index, should not contribute to K_{DP}). They also stated that Z_{DR} of a mixture of rain and hail is completely dominated by the Z_{DR} of the hail (as is the case for Z_H); Z_{DR} they postulated, could provide the necessary information concerning the orientation of the hail. Initially, Balakrishnan and Zrnić proposed an empirical relationship of the form:

$$Z\ (\text{dBZ}) = 49 + 8 \log(K_{DP}) \tag{10}$$

as the boundary to distinguish pure rain from mixed phase and hail, which is clearly in error; for values of K_{DP} above 7° km^{-1} it predicts Z values lower than (9) which is their equation for pure rain. They then suggested that an empirical relationship between the hail/rain boundary was given by a value of Z some 7 dB higher than in (9); this 7 dB offset was to some extent confirmed by Ryzhkov and Zrnić (1994):

$$Z\ (\text{dBZ}) = 51 + 13.86 \log(K_{DP}). \tag{11}$$

Equation (6), based on the Goddard *et al.* (1982) drop shapes, leads to a relationship for rain of the form:

$$Z\ (\text{dBZ}) = 45.2 + 11.2 \log(K_{DP}) \tag{12}$$

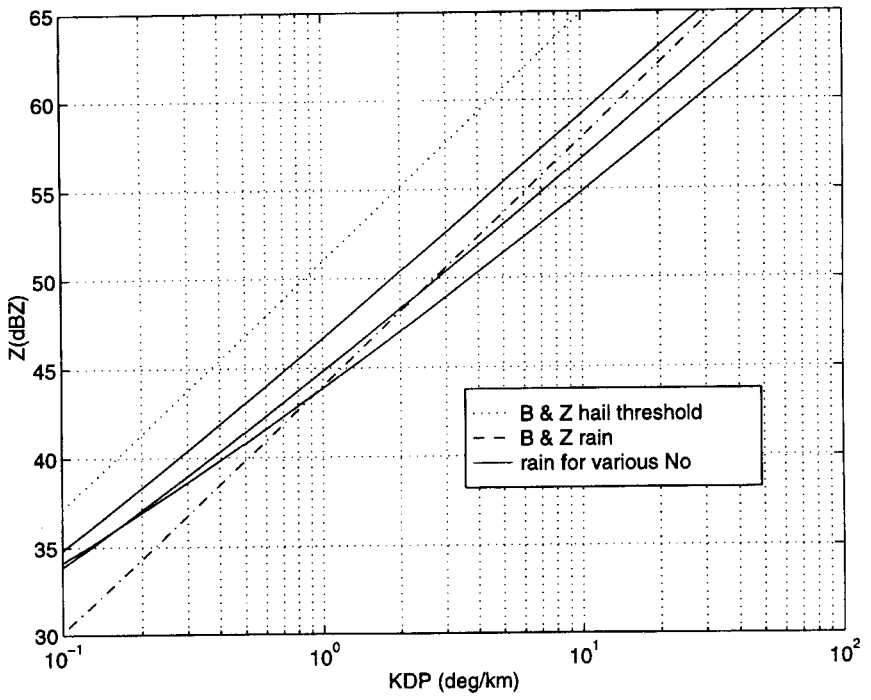

Figure 4. Predicted values of two-way K_{DP} and Z_H for rain and hail. Dash-dot, pure rain; dotted, pure hail (both from Balakrishnan and Zrnić 1990); solid, rain for various values of N_0 using 'new' drop shapes and Eq. (12). See text for definitions and discussion.

for a value of $N_0 = 8000\ \mathrm{m^{-3}mm^{-1}}$. In Fig. 4 are plotted profiles of Z (dBZ) in pure rain from (9) (dash-dot line), together with the additional 7 dB hail-threshold curve from (11) (dotted line) and also (12) (solid line). Earlier we pointed out that the exponent 1.37 in (7) based on the 'new' drop shapes leads to a relationship of K_{DP} to R which is more sensitive to the value of N_0 for the drop spectra. In Fig. 4 the three solid lines are for values of N_0 of 800 (upper), 8000 (mid) and 80 000 (lower) $\mathrm{m^{-3}mm^{-1}}$; these factor-of-ten ranges encompass the natural variability of the observed values of N_0 in rain (e.g. Waldvogel 1974). This figure confirms the degree of uncertainty in the precise identification of hail from simultaneous observations of Z and K_{DP}.

Aydin *et al.* (1995) demonstrated the capability of K_{DP} for estimating rainfall rates in a severe storm with rainfall accompanied by hail (diameter 15–20 mm). Using relationships of K_{DP} to R they found remarkably good agreement between the radar and *in situ* rain-gauge measurements. The accumulated rainfall was within 10% of the radar estimates, showing that K_{DP} is effective for estimating R in the presence of hail.

Large hailstones make a negligible contribution to the propagation component of ϕ_{DP} but, if wet, the contribution of differential-phase shift on backscatter, δ, can have a large but transient effect on ϕ_{DP} (Figs. 1 and 2). Hailstones may attain such a size as to produce backscatter effects in the Mie regime even at S-band. This then would invalidate the assumption that the value of ϕ_{DP} is attributable entirely to the propagation component K_{DP}. Melting hail can produce differing effects on the various radar parameters. Aydin and Zhao (1990), in a theoretical study, predicted that well oriented, partially melted hailstones of moderate size (about 30 mm) could produce low positive Z_{DR} combined with large transient increases in the observed ϕ_{DP} due to pronounced Mie effects. In an observational

study using both the WSR-88D radar and the nearby dual polarization radar at Cimarron (Colorado, USA), Zrnić *et al.* (1993) used δ to categorise hail size. δ fluctuates rapidly and changes sign over a narrow size band. They observed a persistent negative δ feature, and attributed it to horizontally oriented water coated oblates of size between 8 and 16 mm. It must be noted here that δ is very sensitive to changes in the composition of the hailstones.

Zrnić *et al.* (1993) assumed δ was transient and could be removed by filtering, which then left a standard error of 3–5° in the derived value of ϕ_{DP}. K_{DP} is the derivative of ϕ_{DP} and so becomes quite noisy, especially when attempts are made to estimate it over short distances. These uncertainties can make it difficult to apply (10), (11) and (12) in practice.

3. Hailstone fall mode

Knight (1986) stated that the tumbling motion determines the average orientation of the long dimension, be it in the vertical, the horizontal or a random direction. This in turn would have an effect on the polarization on backscatter of the radar signal. The fall mode of hailstones is therefore of crucial importance in the polarimetric radar detection of hail, and it is an area where there is little consensus of opinion.

Bringi *et al.* (1984) and Aydin *et al.* (1986) assume that the hail medium is isotropic. This is consistent with the findings of Knight and Knight (1970) who, in their detailed examination of the behaviour of falling hailstones, concluded that oblate hailstones tumble rapidly as they fall and grow with no strong orientation effect. Using circular polarization radar, Hendry and Antar (1984) showed that the degree of common alignment of hail is generally much smaller than that of rainfall.

Hailstones display a wide variety of shapes, which implies that there are a great number of different fall modes. The most common shape is that of an oblate spheroid (Browning and Beimers 1967). These 'oblates' even display a degree of triaxiality (Thwaites *et al.* 1977). Thwaites *et al.* found that the ratio of the major to minor axis was between 0.3 and 1, the mean value being between 0.6 and 0.8. Large oblate hailstones could produce a considerable departure from the hail signatures of Bringi *et al.* (1984) and Aydin *et al.* (1986) if they were preferentially oriented.

Zrnić *et al.* (1993) assumed that both large oblate and prolate hailstones would tend to be vertically oriented, i.e. have vertical fall mode, that is with the minor axis in the horizontal; they speculated that hail with diameters larger than about 2 cm would produce Z_{DR} values of around -1 dB. Illingworth *et al.* (1987) reported one example of a region of negative Z_{DR} of about 1 km in depth at a height of 5 km with values down to -1 dB, which was coincidental with the 60 dBZ contour, but it was very transitory and only lasted a few minutes. Negative values of Z_{DR} imply that the hail has a vertical fall mode. This is consistent with the theoretical calculations of Kry and List (1974); they termed one class of solution symmetric gyration. Thwaites *et al.* (1977) considered this to be the most general fall mode of hailstones, and used it as a basis for their experimental work. They grew artificial hail with a similar shape and structure to that of natural oblate hail by attaching a spherical embryo to a rotating axle and, at the same time, causing the minor axis to move in a conical manner about the horizontal. They inferred that if naturally oblate hail grows during this type of motion, triaxiality could be produced using elliptical rather than a symmetrical cone of motion. In the limiting case the minor axis would be in the horizontal and hence produce the negative values of Z_{DR}.

List (1959) carried out experiments in a water tank using oblate spheroids. He concluded that oblate hail falls with the shortest axis vertical, acquiring maximum drag and minimum speed. This would lead to positive values of Z_{DR}. Browning and Beimers (1967) argued that if this fall mode continued, then the resulting hailstone growth would very

quickly become asymmetric, this being contrary to observation. They postulated that symmetry is preserved by the hailstone occasionally flipping over, although Knight and Knight (1970) stated that to produce such excellent symmetry as is often observed the hailstones would have to flip very quickly. Oblate hailstones oriented in the manner described here would give a positive value of Z_{DR} and, depending upon the degree of oblateness and size of the hailstones, would if wet produce a differential-phase shift on backscatter (δ). This would only be manifested, though, if the hail medium throughout the pulse volume had a preferred orientation (e.g. McCormick *et al.* 1979).

4. Observations

We report on coincidental multi-parameter-radar and *in situ* measurements of the precipitation produced by a summer hailstorm that developed and grew in southern England on 10 June 1995. The hailstorm was remotely sensed by the S-band ($\lambda = 9.75$ cm) Chilbolton radar which has Doppler and polarization capability (Goddard *et al.* 1994a) and a narrow (0.28°) beam width, allowing excellent resolution of the storm structure.

The hailstorm formed in conditions favouring vigorous convection. The maximum temperatures in the area were around 30 °C, and a nearby upper-air ascent revealed considerable instability aloft favouring conditions for deep convection. The adiabatic liquid water content (LWC) was calculated from the ascent and found to be 14 g m^{-3}. Both high LWC and strong vertical updraughts are important factors in the production of large hall (e.g. List 1985).

The storm was tracked for about 30 minutes (between 1700 and 1730 UTC) roughly corresponding to a track 10 km long, starting about 15 km to the south-west of the town of Reading (Berkshire) and moving through its western districts and then north and east. The storm moved at 20 km hr^{-1} in a broadly northerly direction, although individual cells had a more north-easterly trajectory.

The radar data were coincidental with ground *in situ* verification of the presence of hail by more than 80 observers in the Tilehurst area of Reading, and by the collection of 55 hailstones. This aided the interpretation of the various radar parameters and has allowed various hail-detection algorithms to be tested. The hailstones were transported to a cold room so that structural descriptions and measurements of size and degree of oblateness could be made. Closer examination of the radar data has allowed an insight into the fall mode of the hailstones, which is a determining factor in their resulting shape.

(*a*) *Ground truth hail observations*

Figure 5 shows the ground observations of hail which extended in a swath about 20 km long and around 3 km wide, although the exact extent would be hard to verify as the areas to the west and south of Calcot are more sparsely populated. Hail-only observations (a period during the storm's passage over the observation point where the precipitation was purely hail) were located on the eastern edge of the storm. In this region observers reported the hail to be larger than that observed further west, and shaped like lozenges or discs. Satellite and radar observations showed that the storm moved in a north-north-easterly direction, so the map gives a time integrated picture; the hail was observed in Burghfield some 20 minutes before it reached the Tilehurst environs. Disc-shaped hail was also reported at Burghfield and specimens were saved for analysis. The general storm sequence over Tilehurst (apart from the eastern fringe) was a period of torrential rain followed by a fall of large disc-shaped hail and then another period of rain. The whole sequence lasted between 10 and 15 minutes. Damage was reported at several locations. Holes were made in corrugated plastic roofing where the hail had attained sufficient size

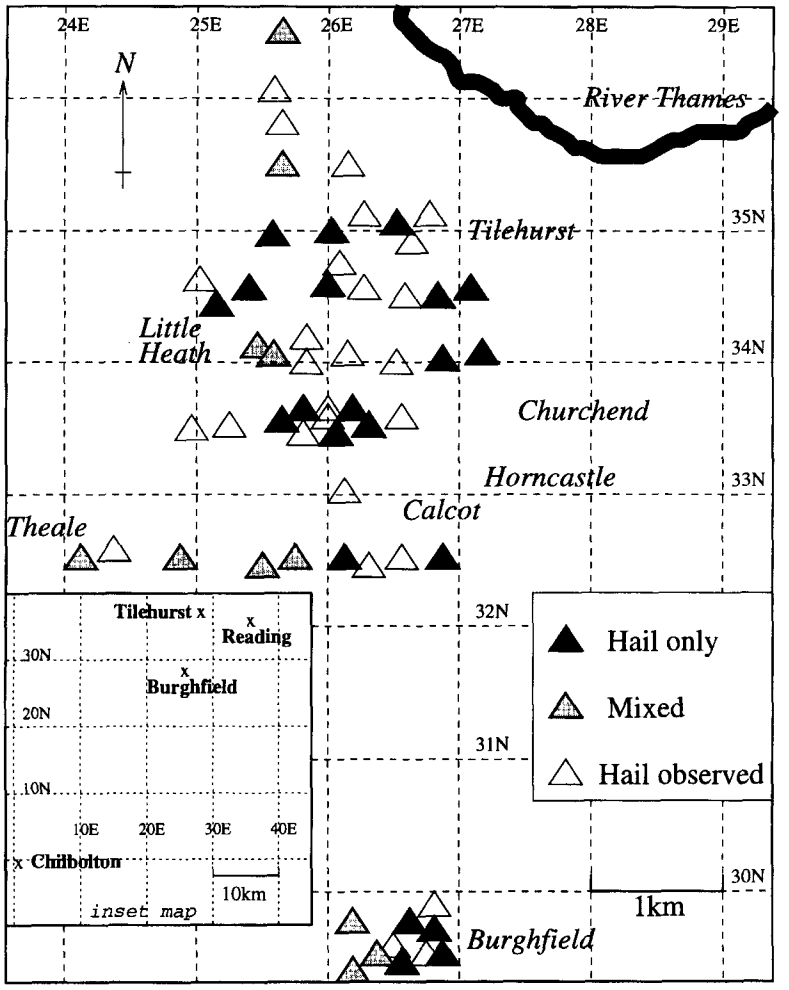

Figure 5. Map of the hail observations made between 1700 and 1730 UTC 10 July 1995. The distances north and south (km) are relative to the Chilbolton radar (51.145°N, 1.437°W).

and terminal velocity. Cars were also dented and leaves stripped from plants and trees. Photographic evidence of hail lying on the ground shows that there was a remarkably low number concentration ($N \sim 100$ m^{-2}) which ground-based observers confirmed fell in a period of 5 minutes with no accompanying rain.

Fifty-five hailstones were collected from Burghfield (see Fig. 5). Upon measurement in a cold room, they were found to be similar in dimensions and shape to those observed at Tilehurst. Figure 6 is a photograph of one of the hailstones collected, it has been cut in half so that the interior can be examined more closely. The hailstone is oblate rather than prolate, and contains a well-defined approximately circular embryo surrounded by several growth rings from alternate wet (transparent ice) and dry (milky ice) growth regimes (Johnson and Rasmussen 1992). The hailstone shown represents the typical size observed during this storm, being 2.2 cm along the major axis with an axial ratio (major to minor) of 0.6. The largest hailstones measured had a major axis of 3.2 cm. The structure of the hailstones was remarkably similar, suggesting that they originated and passed through the same regions of the storm. Wet growth was also apparent in regions of cloudy ice in some hailstones. We

Figure 6. Cross sectional photograph of a hailstone (enlarged to show detail) collected at Burghfield Common. See text for further details.

speculate that this occurs when unfrozen water is built into, and stabilised by, the growing ice framework, with the rate of heat transfer being insufficient to freeze the large quantities of supercooled water collected.

(*b*) *Radar observations*

For the radar observations we focus on a single Plan Position Indicator, PPI, (1720 UTC) which best captures the relevant differential-scattering signatures in the lower levels of the storm in plan view. We will also focus on two particular rays (with azimuths 37.8° and 29.38°) in the storm, to quantitatively interpret the scattering signatures.

(i) *Guide to significant features of PPI.* Figure 7 shows a radar PPI within a minute or so of the time of the hail observations in the Tilehurst area, 27 km east and 35 km north of the radar (henceforward 27E 35N). The height of the radar cross-section at a range of 45 km is 700 m, 2.3 km below the melting layer.

The area where $Z_{DR} > 3$ dB tends to follow the 50 dBZ contour as would be expected for heavy rain, but where $Z > 60$ dBZ at 26E 34N, Z_{DR} dips below 2 dB; if this were pure rainfall the low value of Z_{DR} implies an unrealistic rainfall rate of $\sim$1000 mm hr^{-1}, thus we infer the presence of mixed rain and tumbling hail. The Z_{DR} does not drop to zero, which would be indicative of purely tumbling hail, but instead either the hail component has some degree of alignment or the rain component acts to raise the value of Z_{DR}.

The region where the large oblate hail was observed to fall is near 28E 35N. Here Z_{DR} is about $3 \rightarrow 5$ dB. This suggests that the oblate hailstones were not randomly tumbling as they fell, but rather had a systematic fall mode with their major axes in the horizontal. Here Z_H is between 40 and 60 dBZ, which is consistent with the low number density of hailstones observed at the ground, given their exceptional size.

As we use an internally consistent (reflectivity) calibration technique that assumes a pure rain medium, we must identify a part of the scan where we are confident of rain-only echoes. The precipitation in the north-west quadrant of Fig. 7 is all rain, as confirmed by the values of LDR below -28 dB, and the monotonically rising ϕ_{DP} giving two-way K_{DP}

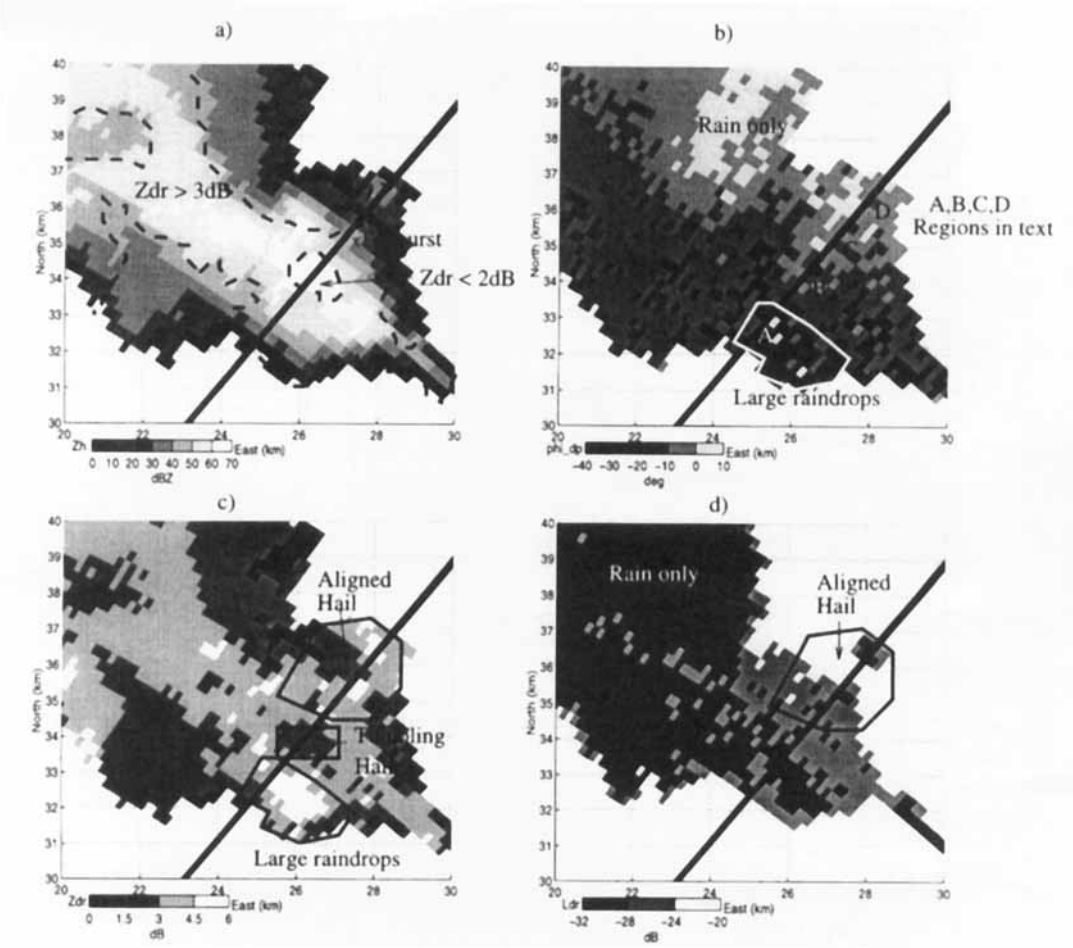

Figure 7. PPI of storm showing (a) Z_H; (b) Z_{DR}; (c) ϕ_{DP} and (d) LDR, at 1720 UTC 10 July 1995 with elevation 0.7°. The bold line shows the ray profile of Fig. 8; Tilehurst is positioned 27 km east and 35 km north of the radar. See text for further details.

values in the heaviest precipitation of about 16° km^{-1}, indicating rainfall rates of nearly 200 mm hr^{-1}. Range profiles through this region were used for the absolute calibration of the radar (see Fig. 10; this is discussed in section 5).

(ii) *Ray profile through hail-bearing regions.* The observations in the eastern half of Fig. 7 are more complicated, as the ray profile in Fig. 8 demonstrates. The ϕ_{DP} profile was generated by taking the mean of four separate rays through the region containing hail. As each ray has a beam width of 0.28°, this results in a sample width of nearly 1 km at the range of the hailstorm. Using this method, the noise in ϕ_{DP} is reduced and the equivalent of a 1 second dwell is obtained (calculated from the slew rate of the dish).

The small region at 26E 32N ('A' in Fig. 8), where ϕ_{DP} falls 7 → 10° (see Fig. 2) below the system value of −27° and Z_{DR} exceeds 5 dB, cannot be a propagation effect, but must be due to differential-phase shift on backscatter. This is consistent with monodispersed 7 → 8 mm diameter raindrops which have very little canting, a conclusion confirmed by the low value of LDR. Region B in Fig. 8 exhibits the classic signature of a Z_{DR} 'dip' due to tumbling hail (or conceivably hail with a degree of alignment) mixed with rain.

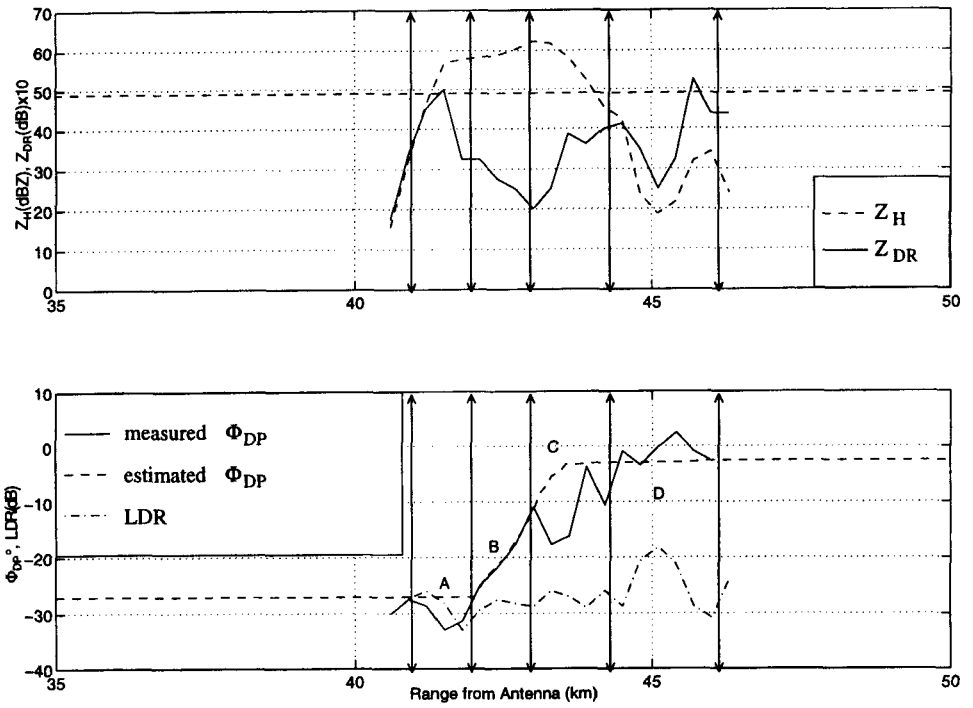

Figure 8. Ray profiles of the radar parameters along the bold line in Fig. 7 at 1720 UTC 10 July 1995 with elevation 0.7°.

Region C is the region centred on 28E 36N in Fig. 7 where ϕ_{DP} becomes noisy, and is coincident with the ground observations of oblate hail. LDR has risen somewhat and Z_{DR} is between 2 and 4 dB; this strongly suggests oblate hailstones large enough to undergo Mie scattering, with a spread of canting angles to give the observed LDR. The lower Z_H value in a region of large hailstones is consistent with their low concentration (Mie scattering would reduce Z_H further). Such a low concentration cannot produce significant K_{DP}, so we interpret the total differential-phase shift values as local deviations superimposed on a trend (increasing phase difference), indicating large negative values of δ ($-10°$) due to wet oblate hail, with a degree of alignment (Fig. 1). Because of the very narrow radar beam width it is unlikely that reflectivity gradients are degrading the phase measurements.

In region B in Fig. 8, and by extrapolation the first half of region C, the value of K_{DP} is 14° km^{-1} (indicating a rainfall rate of about 180 mm hr^{-1} from (5) or (7)) accompanied by values of Z_H which are close to 60 dBZ. Figure 4 and (9) would predict the rain component having a value of Z_H close to 60 dBZ; however, (12) suggests a slightly lower value of Z_H, but if the rain has N_0 of 800 or 80 000 m^{-3}mm^{-1} the values could be 62 and 57 dBZ respectively. This uncertainty in the values of Z_H for a given rainfall rate highlight the difficulties of using (11) as a hail criterion. In this case to trigger the algorithm Z_H would need to be >67 dBZ, yet the low values of Z_{DR} observed clearly indicate the presence of hail. For pure rain, a rainfall rate of 180 mm hr^{-1} and a Z_H of 60 dBZ should be accompanied by Z_{DR} values of 3.5 dB.

In region D in Fig. 8, LDR rises to -18 dB which is indicative of wet oblate hail; Z_{DR} has values of 2–3 dB, which is consistent with an aligned fall mode with the major axis on average in the horizontal with 20° canting angle (for an axial ratio of 0.6). Because LDR at the back of the storm reverts to -30 dB, we feel that these LDR observations are

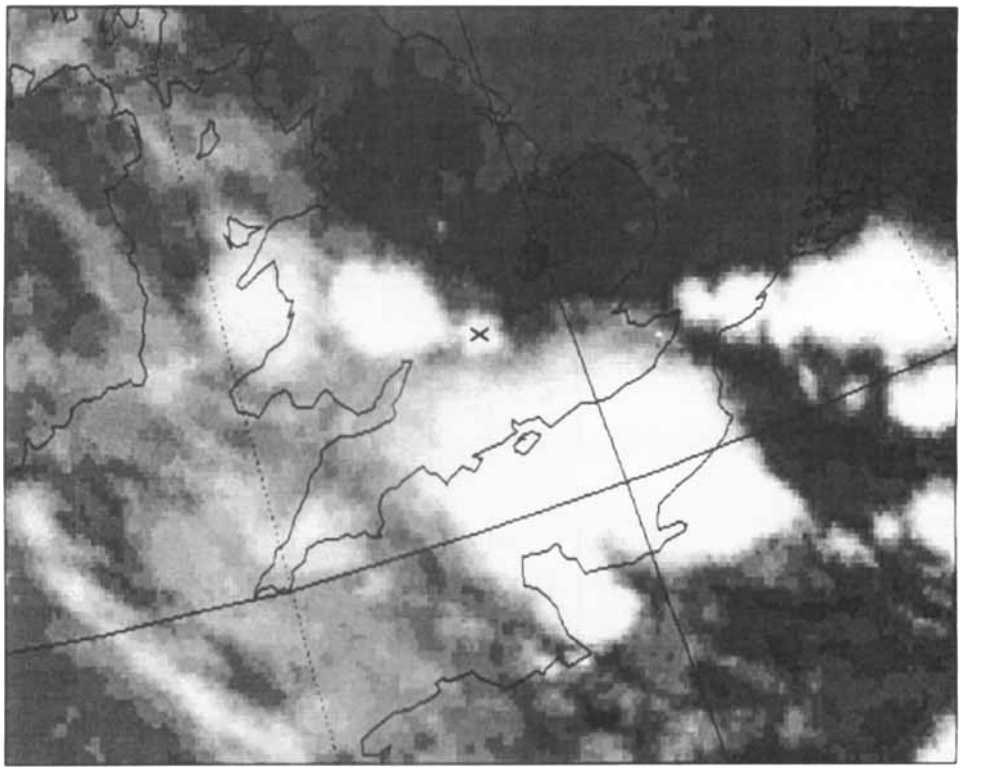

Figure 9. Meteosat infrared image for 1700 UTC 10 July 1995.

unaffected by propagation and depolarization of the incident beam. The value of K_{DP} is negligible, which suggests that rain was not mixed with the hail and, indeed, the ground-based observations in this region (Fig. 5) consistently reported a period with only hail falling and the hailstones being exceptionally large and oblate. The hail is wet because the air temperature is above 0 °C.

We are suggesting that region D contains hail, but it is rather difficult to apply the hail criterion of Balakrishnan and Zrnić (1990) in this region because δ leads to an uncertainty in the value of K_{DP}. If K_{DP} is 0.1° km^{-1} or 1° km^{-1} then (11) predicts hail if $Z_H > 37$ and 51 dBZ respectively. The observed Z_H is lower than either of these two values.

(*c*) *Satellite observations*

The available Meteosat infrared image closest in time to the observations is at 1700 UTC (Fig. 9; the hailstorm's position is marked with a cross). The minimum cloud-top temperature, which is indicative of the greatest altitude of the storm at this time, is −56 °C (the lowest temperatures are −60 °C). For the Hardaker and Auer (1994) hail algorithm to be triggered, a coincidental reflectivity of 55 dBZ is required. The UK networked radar situated at Chenies (51.68°N, 0.53°W), which has a 2 km grid resolution, showed a maximum reflectivity of 56 dBZ at this time, although determining whether or not the 55 dBZ radar and −56 °C satellite pixels are exactly coincidental is problematic. This is because the cloud casts a 'shadow' in the infrared satellite image. The distance between the actual and apparent positions of the cloud is a function of both the cloud-top height and the viewing angle of incidence (latitude and longitude dependent) by the satellite's

radiometer. In addition, wind shear may displace the cold cloud top from above the main precipitation core. The most important function of a hail-detection algorithm is to pinpoint the hail. With this method it is only possible to say that there is an increased probability of hail falling somewhere within the storm cell, this region being diagnosed by the low cloud-top temperatures and high reflectivity.

5. Derived rainfall rates

Figure 10 shows a ray profile through the rain in the north-west quadrant of the storm shown in Fig. 7. The parameters shown are the measured and predicted total ϕ_{DP} along the path predicted using the calibration method of Goddard *et al.* (1994a). The effect of adding/subtracting 1 dBZ of power from Z_H on the expected K_{DP} is shown. Figure 11 (from Goddard *et al.* 1994a) is the theoretical basis for the calibration method, and shows that the ratio K_{DP}/Z_H as a function of Z_{DR} only varies very slightly as the integer index, m, of the gamma raindrop size distribution changes. The gamma function is a variation of (6) and takes the form:

$$N(D) = N_0 D^m \exp[-\{(3.67 + m)D\}/D_0] \ (\mathrm{m}^{-3}\mathrm{mm}^{-1}). \tag{13}$$

K_{DP} (specific differential phase) can be predicted from the (non-attenuated) Z_H and Z_{DR} measurements at each radar range gate. Uncertainties about the form of the gamma distribution are relatively unimportant compared with a change in absolute-power calibration of ± 1 dBZ. This method can therefore be used to accurately calibrate Z_H to at least within 0.5 dBZ, especially if long dwell periods are used. (Z_{DR} can be calibrated by using a

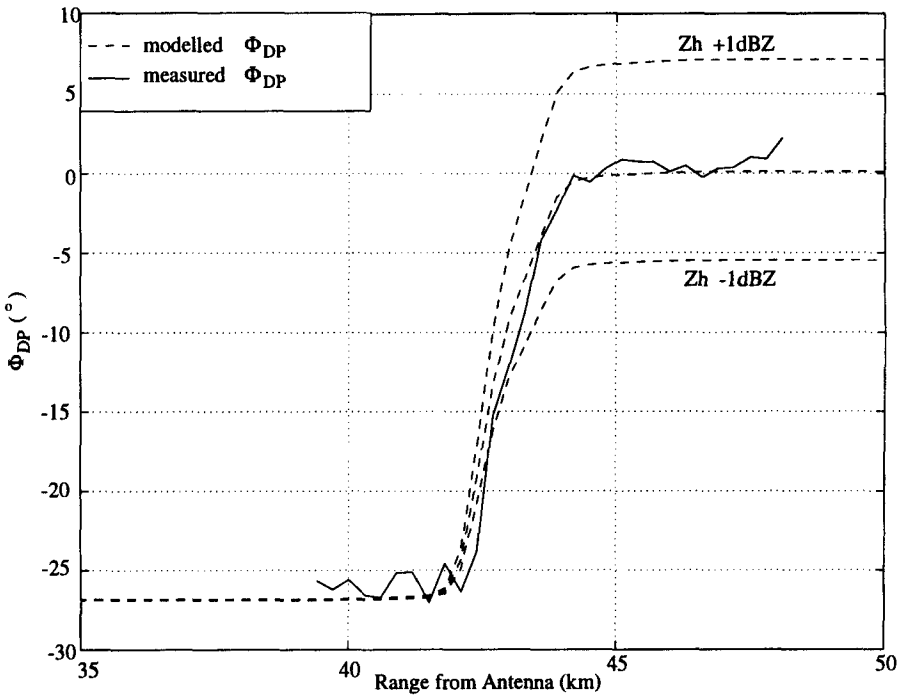

Figure 10. The Goddard *et al.* (1994b) calibration technique applied to a ray through the rainfall in the north-west quadrant of Fig. 7 at 1720 UTC 10 July 1995 with azimuth 31.9° to 32.8°, showing the sensitivity of the computed ϕ_{DP} to small changes in the calibration of Z_H. See text for further details.

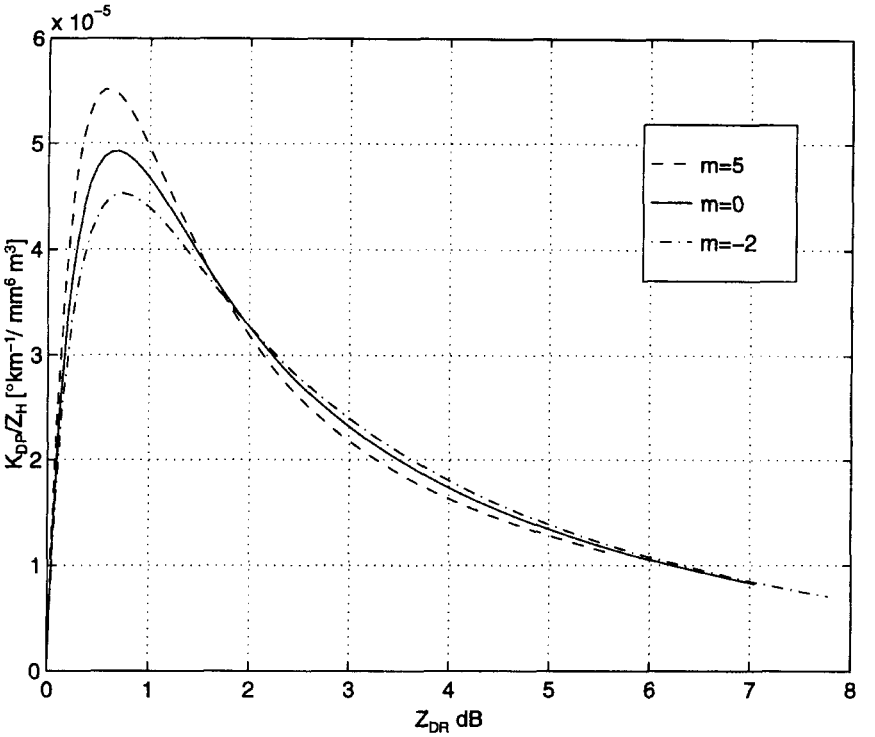

Figure 11. Theoretical variation of K_{DP}/Z_H as a function of Z_{DR} modelled using different values of m within a gamma raindrop size distribution, Eq. (6). See text for definitions and discussion.

Range–Height Indicator (RHI) through the ice phase section of the storm above the melting layer; the values of Z_{DR} at altitudes above the freezing layer within the ice should be very close to 0 dB, any offset from this value can be added or subtracted.) Figure 10 shows close agreement between the measured and expected total ϕ_{DP} along the path, which confirms that the precipitation is rain. It also implies that we can have confidence in the absolute calibration of Z_H.

Algorithms to detect hail within mixed phase precipitation make use of K_{DP} to extract the relative contributions from rain and hail. Figure 12 is a ray profile through a different region of the same storm shown in Fig. 7 some 13 minutes earlier. Figure 8 and Fig. 12 show the importance of δ, which causes ambiguities in the interpretation of ϕ_{DP} purely in terms of K_{DP}. In region 1 in Fig. 12 the precipitation volume is filled with a low number density of large raindrops; in region 2 there is a mixture of rain and tumbling hail. The flat gradient in ϕ_{DP} beyond 40 km in region 4 is indicative of light rain (the positive Z_{DR} indicating a low concentration of large drops) which gives a very slight contribution to K_{DP} and no δ. This provides a fixed point to quantify the total amount of differential-propagation-phase shift that has occurred through the storm. The dashed line on Fig. 12, drawn by eye, represents an estimate of the ϕ_{DP} (propagation) response, starting at the system offset of $-27°$ which was determined from background ϕ_{DP} values in light precipitation. This provides another fixed point, allowing us to deduce that between 37 and 41 km the propagation-phase-shift change due to propagation through the precipitation volume is $+23°$. The difference between the ϕ_{DP} and K_{DP} profiles is caused by a large negative contribution from δ, suppressing the ϕ_{DP} signal and indicating large oblate wet aligned hail in region 3. The difference between the observed ϕ_{DP} profile (solid line) and the extrapolated ϕ_{DP} profile (dashed line) is caused

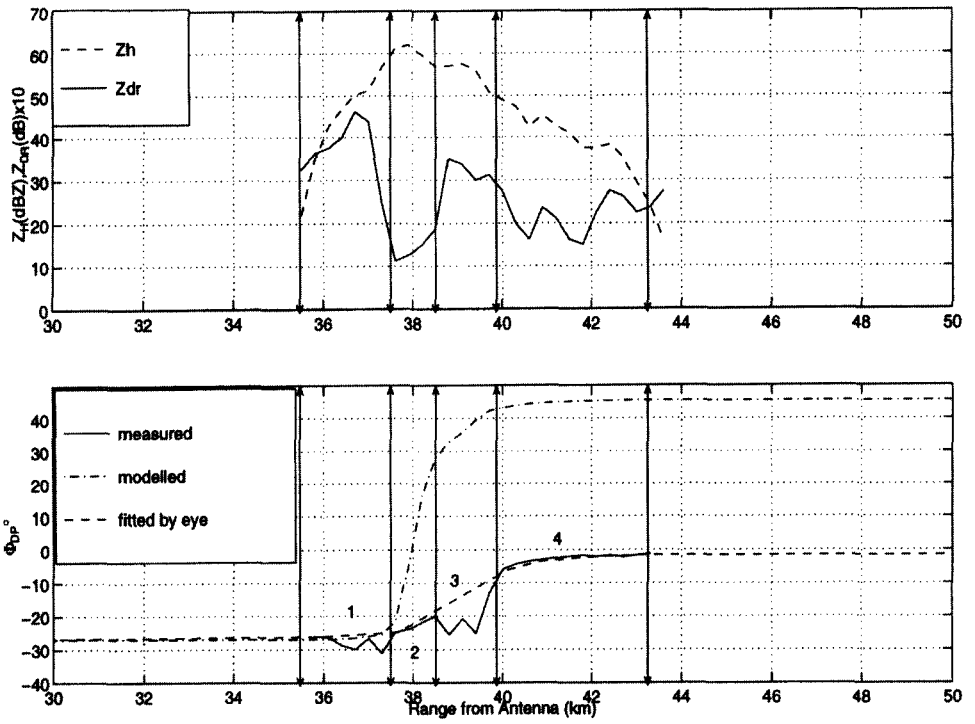

Figure 12. Measured and modelled radar parameters along a ray, azimuth 29.38°, elevation 0.7° at 1707 UTC 10 July 1995. See text for definitions and discussion.

by the large negative contribution from δ indicating large oblate wet hail in region 3. Literal interpretation of the jump in the ϕ_{DP} profile as K_{DP} would predict rainfall rates of 325 mm hr^{-1}; clearly incompatible with the observed Z_H of 50 dBZ at this point. If we take the extrapolated value of K_{DP} between 38 and 40 km range as 8.5° km^{-1}, indicating a rainfall rate of about 120 mm hr^{-1}, then Fig. 4 predicts that Z_H should be between 54 and 58 dBZ depending upon the N_0 of the rain. The observed value is between 58 and 60 dBZ indicating that about half of the echo is probably due to hail. Uncertainties in the value of K_{DP} in the presence of δ limit the precision of this conclusion, but confirmation is provided by values of Z_{DR} below 2 dB, which are too low for pure rainfall of this intensity.

The largest values of δ in Fig. 12 are approximately $-20°$ in region 3, which is consistent with spongy hailstones with a diameter of 20 mm and an axial ratio of 0.5. We therefore postulate that in region 3 hailstones of this composition and with these dimensions are present, masking the propagation component of the total differential-phase shift and causing ambiguity in its interpretation using K_{DP}. Finite δ can only be produced by hydrometeors with a degree of alignment; additionally the positive values of Z_{DR} (~3 dB) imply that the alignment was, on average, with the minor axis in the vertical. This is consistent with the theories of Browning and Beimers (1967) and suggests that the fall mode is anisotropic, rendering the hail 'invisible' to the hail-detection algorithm of Aydin *et al.* (1986).

Our analysis of Figs. 8 and 12 draws attention to the difficulties of deriving rainfall rates and identifying the presence of hail from Z_H and ϕ_{DP}. Two problems arise: firstly the ϕ_{DP} profile can be affected by δ, the differential-phase shift on backscatter; and secondly the relationship between K_{DP} and rainfall rate (and hence K_{DP} and Z_H for rain) is not

unique, but depends on an assumed value of N_0 in the raindrop size spectra. In the next section we shall consider how the variables Z_H, Z_{DR} and K_{DP} can be combined. Because K_{DP} and Z_{DR} in rainfall are not independent, their very dependence and consistency can be used to calibrate Z_H when rain is known to be present. If the consistency fails, then regions where significant hail is present can be identified.

6. New hail-detection algorithm

The calibration method of Goddard *et al.* (1994b) could have an application as a viable method for hail detection, as well as providing an accurate method for calibration. Essentially this calibration technique *assumes* only raindrops are present in the scattering volume, and then relies on the fact that the value of K_{DP}/Z_H is a unique function of Z_{DR} (Fig. 11). The calibration of Z_H is adjusted so that the path-integrated phase shift, calculated from the theoretical value of K_{DP} at each gate derived from the observed values of Z_H and Z_{DR}, agrees with the observed path-integrated phase shift (Fig. 10). The advantage of this approach is that the path-integrated phase shift is used as a constraint and this quantity can be estimated quite accurately. This contrasts with the errors involved in trying to derive K_{DP} from differentiating a very noisy ϕ_{DP} profile. Once the radar is calibrated, then for all paths through rain the integrated phase shift computed from the observed values of Z_H and Z_{DR} should agree with the observed total change in ϕ_{DP} along the path. Any difference between the measured ϕ_{DP} and the predicted value will indicate a violation of the 'rain-only' assumption, and should therefore detect the presence of any non-rain precipitation.

Figure 12 shows the total phase shift (dash-dot line) predicted from the observed values of Z_H and Z_{DR} assuming that only rain is present. The total phase shift is massively overestimated; most of the divergence from observations occurring in region 2 where the values of Z_H are high but Z_{DR} is low. If this region was characterized purely by rainfall with a Z_{DR} of 1.2 dB and $Z_H = 62$ dBZ, it would imply that there was a large concentration of small raindrops with N_0 200 times the Marshall Palmer value, and an implausible rain rate of 1000 mm hr^{-1}. However, the integrated phase shift based on the rain assumption is 50° higher than that observed, confirming that region 2 contains randomly tumbling hail which is depressing Z_{DR} and raising Z_H.

The difference between the observed additional phase shift for each 300 m gate and that calculated from Z_H and Z_{DR} at that gate, assuming rain to be present, is displayed in Fig. 13 for the data along the ray in Fig. 12. The observed ϕ_{DP} is quite noisy, so averages over five adjacent rays, each separated by one degree in azimuth, were taken. This is equivalent to a distance of nearly 1 km at this range. The root mean square (r.m.s.) noise in observed ϕ_{DP} is typically ±2°, and Fig. 13 indicates that if the difference between the observed and computed change in differential-phase shift from one gate to the next is more than 2° then hail is present. In region 2 the theoretical value of the phase shift is greater than that observed by 12°, because hail is depressing the value of Z_{DR}. In region 3 the theoretical value is less than that observed by about 8°; the deviation is negative because the differential-phase shift on backscatter from the large hail is depressing the observed phase shift. This hail algorithm can, therefore, detect hail where other algorithms fail, namely where there is a mixture of rain and hail and also where large oblate hail causes finite δ. As a control, the algorithm was tested in regions of moderately heavy rain ($Z_H > 40$ dBZ and where ϕ_{DP} increased monotonically). The results for a typical rain ray are shown in Fig. 14(a)–(c). The difference between the measured and predicted ϕ_{DP} is less than ±2°, which confirms that there is no hail along the length of the ray.

Finally, in Fig. 15 the hail-detection algorithm is applied to the PPI data in Fig. 7. In this figure we have plotted the difference between the theoretical path-integrated

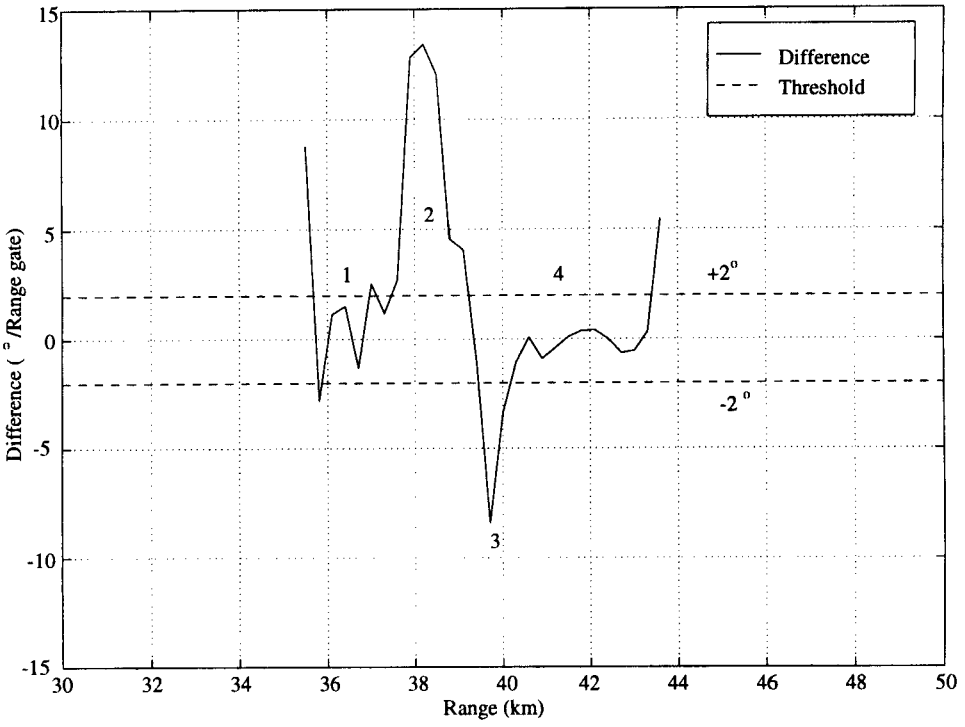

Figure 13. Difference between the gradients in modelled and measured ϕ_{DP} for the ray shown in Fig. 12.

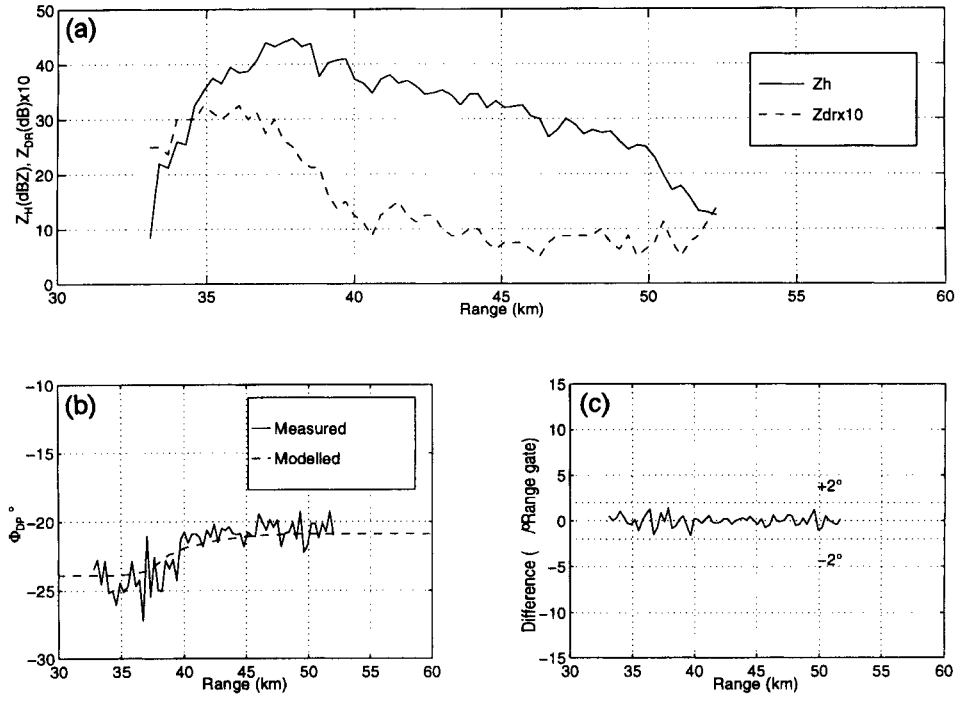

Figure 14. Ray through a region of rain, at 1707:37 UTC 10 July 1995, azimuth 13.4°. (a) Z_H and Z_{DR}; (b) measured and modelled ϕ_{DP}; (c) difference between the gradients of modelled and measured ϕ_{DP}.

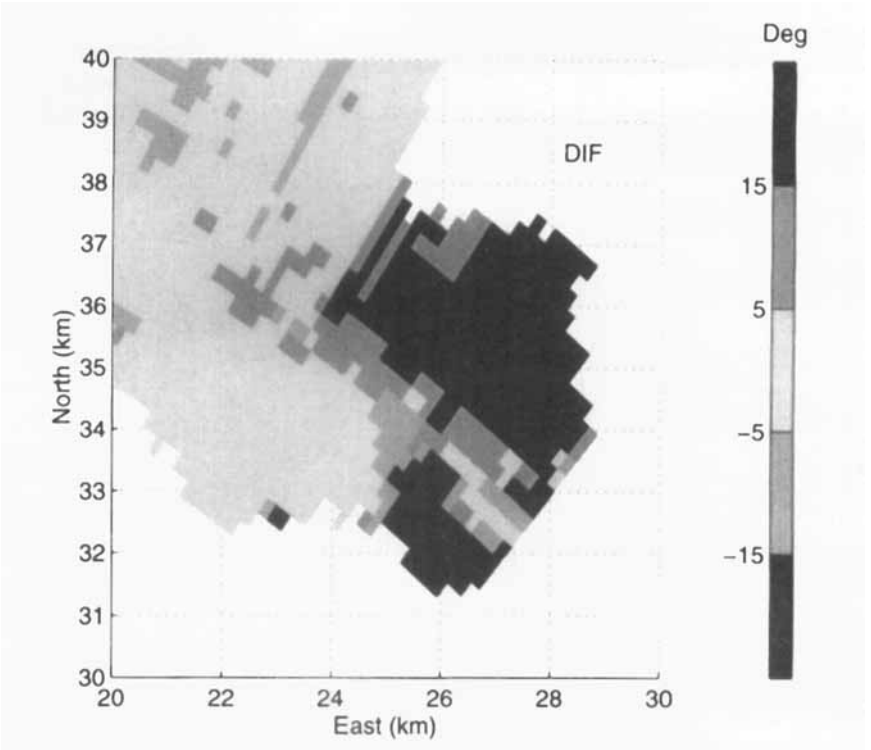

Figure 15. Performance of the new hail-detection algorithm for the PPI data in Fig. 7. The variable plotted is the difference in the value between ϕ_{DP} along radar rays computed from Z_H and Z_{DR}, assuming rain is present, and the observed value of ϕ_{DP} along the ray. Where hail is present this difference changes by more than 5° km^{-1}, but in the rain in the north-west quadrant the difference stays below 5°.

differential-phase shift assuming rain and the observed differential-phase shift. In the north-west quadrant the difference is nearly always less than 5° indicating rainfall, whereas in the centre of the plot the difference rapidly increases with range reaching values in excess of 30° behind the hail region. The area deemed to be large raindrops, which are accompanied by a negative value of δ, shows up as a negative difference between theoretical and observed phase difference of more than 15°. In Fig. 15 four adjacent rays have been averaged giving a radial resolution of 1 km. In Figs. 13 and 14 the differences between theoretical and observed phase shift for every 300 m gate were computed. For reliable detection, Fig. 15 indicates that it is probably more realistic to use changes of more than 5° between theory and observation occurring over ranges of 1 km as an indication of the presence of hail.

7. Conclusions

This paper has addressed the question of hailstone fall mode, as this is of crucial importance in the detection of hail by radar. It is likely that many fall modes exist for hailstones, these being both dependent upon, and a determining factor in, their resulting shape and size. The fall mode is forced in turn by the ambient meteorological conditions such as LWC and updraught speed. The established hail-detection algorithm of Aydin *et al.* (1986) is reliant upon the hailstones tumbling randomly, resulting in near-zero values of Z_{DR}, for them to be distinguishable from rain. The oblate hailstones observed in the 10 July 1995 storm fell with their major axis in the horizontal (on average) resulting in

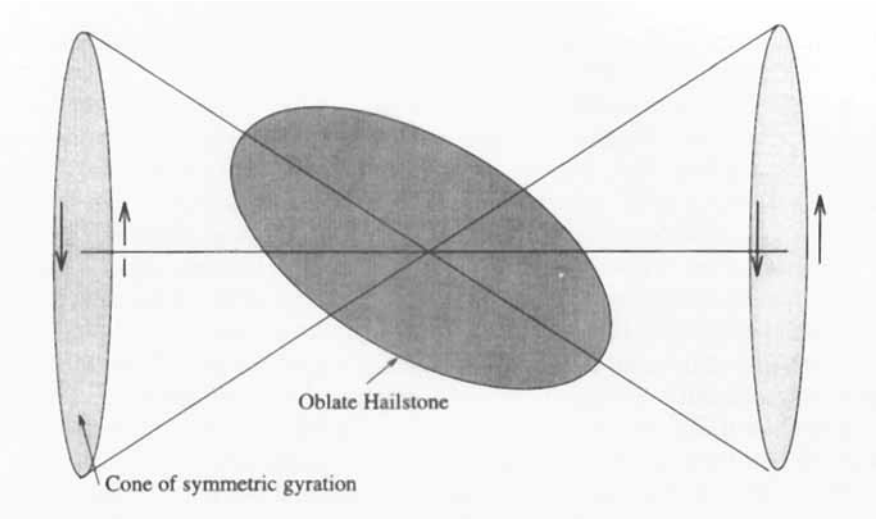

Figure 16. Tumbling motion of an oblate hailstone viewed side on.

$Z_{DR} \sim 3$ dB and causing the hail-detection algorithm to fail. An additional complication is the presence of rain, which also contaminates the Z_{DR} signal. This implies that the hailstones had a preferred orientation as they fell, which raises the additional question of how did the hail fall if it did not tumble randomly?

The radar observations are consistent with the oblate hail falling with its largest axis in the horizontal, implied by high values of Z_{DR}, and canting at $\pm 10 \rightarrow 20^{\circ}$ about the horizontal, deduced from LDR. To be consistent with the radar observations, a possible fall mode would be one where the major axis is describing a cone about the horizontal. This is shown in Fig. 16, and is consistent with the fall mode postulated by Browning and Beimers (1967). To produce the observed hailstone structural symmetry, then the hailstone would have to occasionally flip over to allow the supercooled water to accrete on the opposite face of the stone. An alternative fall mode could involve the hailstones rotating about their major axis, which would result in symmetry. The resulting hailstones would be prolate, though, rather than having the oblate shapes that were observed, i.e. more like a cigar than a disc, so this mode can be rejected.

In the laboratory experiments of Thwaites *et al.* (1977) hail was grown similar in shape and size to that observed on 10 July 1995, but the fall mode they used to grow the hail is inconsistent with the observed radar response. Their fall mode involved the major axis being, on average, in the vertical which would result in negative Z_{DR}.

The hail-identification algorithm of Balakrishnan and Zrnić (1990) relies on converting the observed K_{DP} into a reflectivity component of the rain; if the observed reflectivity is much higher than this, then the difference is due to the presence of hail. In practice difficulties arise. Using the 'new' drop shapes of Goddard *et al.* (1995) it seems that the conversion from K_{DP} to Z_H is dependent on the value of N_0 in the raindrop size spectrum. If we assume that the value of N_0 can vary up and down by a factor of ten, from as low as 8000 up to 80 000 $m^{-3}mm^{-1}$, then this introduces an error of a factor of two (3 dB) in the Z_H value. This uncertainty means that up to 50% of the echo could be due to hail, but would remain undetected. Balakrishnan and Zrnić (1990) suggested that values of Z_H 7 dB above the value predicted for rain from K_{DP} could be used to identify hail; but this leads to such extremely high values of Z_H that our results indicate it would be rarely triggered, even

when the presence of hail is confirmed by ground observations. In addition the derivation of K_{DP} from a noisy ϕ_{DP} profile observed along a ray is error prone, and is affected by a superposed ϕ_{DP} signal due to differential-phase shift on backscatter when the hail is large enough to undergo Mie scattering. Filtering can be used to remove the more obvious spikes due to differential-phase shift, but this is complicated for extensive regions of large hail.

We suggest that a more reliable approach is to use the consistency of the three observables Z_H, Z_{DR} and K_{DP} in rain. This has been proposed as a calibration technique for rain by Goddard *et al.* (1994b) and relies on the fact that, for rain, K_{DP}/Z_H is a unique function of Z_{DR}. In rain the total differential-phase shift found from the theoretical values of K_{DP} at each gate, derived from the observed values of Z_H and Z_{DR}, should agree with the observed value of the total differential-phase shift along the path. If the theoretical and the observed phase shifts diverge, then hail is present. An examination of the Chilbolton data suggests that if five rays are averaged and ranges of 1 km are considered, then a difference in the observed and the calculated differential-phase shift of greater than 5° should be a reliable indicator of the presence of hail. This method has the advantage that it does not rely on deriving a value of K_{DP} by differentiating a noisy profile of differential phase with range. Instead, it compares the observed total phase shift with one computed from observed values of Z_H and Z_{DR}.

We have suggested that hail algorithms which rely on Z_H/Z_{DR} alone can fail because hail may not tumble randomly and can be associated with finite values of Z_{DR}. The new algorithm proposed in this paper could fail if the shape and degree of alignment of the failing hail is precisely matched so that a combination of rain and hail gives the same triplet values of Z_H, Z_{DR} and K_{DP} as would be observed for rain. We have been unable to find such a combination, but it is conceivable that one could occur on very rare occasions. A more serious problem arises due to the contamination of ϕ_{DP} by ground clutter. If 12% of the signal power is due to ground clutter, then the error in Z_H and Z_{DR} will be less than 0.5 dB and virtually negligible. However, because the ground clutter has random phase if we consider the amplitude of the return signal, a 6% component with random phase will introduce a noise of over 3° to ϕ_{DP}. Accordingly, profiles with random gate-to-noise above this level will indicate clutter contamination and should not be used for the hail-detection algorithm.

In conclusion we also note that many operational radars in Europe operate at C-band. The algorithm outlined in this paper should operate reliably at S-band, but at C-band attenuation and propagation problems need to be considered. The values of Z_H will be reduced at the far side of the storm if heavy rainfall is encountered along the ray. In addition, differential attenuation by raindrops leads to reduced values of Z_{DR} at the back of the storm so that they become negative. These propagation effects at C-band are a problem for all proposed hail-identification algorithms which rely on polarization parameters; further work is needed if the new algorithm presented in this paper is to be used at C-band.

Acknowledgements

This work was supported by NERC 'HYREX' grant GST/02/718. We thank the RCRU group at RAL for allowing access to the Chilbolton radar. Jothiram Vivekenanden (NCAR) provided the scattering code. Thanks to Mr. I. Maclean from the University of Reading Library Photographic Services for the hailstone pictures and to Steve Woolnough for spending a whole day at −27 °C measuring hailstones! Thanks to Chun-Lei Liu for the production of Fig. 15.

REFERENCES

Atlas, D. and Ludlam, F. H. 1961 Multiwavelength radar reflectivity of hailstorms. *Q. J. R. Meteorol. Soc.*, **87**, 523–534

Aydin, K. and Zhao, Y. 1990 A computational study of polarimetric radar observables in hail. *IEEE Trans. Geosci. Remote Sens.*, **28**, 412–422

Aydin, K., Seliga, T. and Balaji, V. 1986 Remote sensing of hail with a dual linear polarisation radar. *J. Clim. Appl. Meteorol.*, **25**, 1475–1484

Aydin, K., Bringi, V. N. and Liu, L. 1995 Rain rate estimation in the presence of hail using S-band specific differential phase and other radar parameters. *J. Appl. Meteorol.*, **34**(2), 404–410

Balakrishnan, N. and Zrnić, D. S 1990 Estimation of rain and hail in mixed-phase precipitation. *J. Atmos. Sci.*, **47**, 565–583

Beard, K. V. and Chuang, C. 1987 A new model for the equilibrium shape of raindrops. *J. Atmos. Sci.*, **44**, 1509–1524

Blackman, T. M. and Illingworth, A. J. 1994 Improved measurements of rainfall using differential phase techniques. Pp. 662–671 in *Cost 75 Weather Radar Systems*. EUR 16013. European Commission, Brussels, Belgium

Bringi, V. N., Seliga, T. A. and Aydin, K. 1984 Hail detection with a differential reflectivity radar. *Science*, **225**, 1145–1147

Browning, K. A. and Beimers, J. G. D. 1967 The oblateness of large hailstones. *J. Appl. Meteorol.*, **6**, 1075–1081

Cheng, L. and English, M. 1983 A relationship between hailstone concentration and size. *J. Atmos. Sci.*, **40**, 204–213

Goddard, J. W. F., Cherry, S. M. and Bringi, V. N 1982 Comparison of dual-polarization radar measurements of rain with ground-based distrometer measurements. *J. Appl. Meteorol.*, **21**, 252–256

Goddard, J. W. F., Eastment, J. D. and Thurai, M. 1994a The Chilbolton advanced meteorological radar: a tool for multidisciplinary research. *Electron. & Commun. Eng. J.*, **6**, 77–86

Goddard, J. W. F., Tan, J. and Thurai, M. 1994b Technique for calibration of meteorological radars using differential phase. *Electron. Lett.*, **30**, 166–167

Goddard, J. W. F., Morgan, K. L. Illingworth, A. J. and Sauvageot, H. 1995 'Dual-wavelength polarisation measurements in precipitation using the CAMRA and Rabelais radars'. Pp. 196–198 in Proceedings of the 27th conference on radar meteorology, Vail, Colorado. American Meteorological Society, Boston, USA

Green, A. W. 1975 An approximation for the shape of large raindrops. *J. Appl. Meteorol.*, **14**, 1578–1583

Hardaker, P. J. and Auer, A. H. 1994 The separation of rain and hail using single polarisation radar echoes and IR cloud-top temperatures *Meteorol. Appl.*, **1**, 201–204

Hendry, A. and Antar, Y. N. M. 1984 Precipitation particle identification with centimeter wavelength dual-polarisation radars. *Radio Sci.*, **19**, 115–122

Illingworth, A. J., Goddard, J. W. F. and Cherry, S. M. 1987 Polarization radar studies of precipitation development in convective storms. *Q. J. R. Meteorol. Soc.*, **113**, 469–489

Jameson, A. R. 1983 Microphysical interpretation of multi-parameter radar measurements in rain: Part I interpretation of polarisation measurements and estimation of raindrop shapes. *J. Atmos. Sci.*, **40**, 1792–1802

Johnson, D. B. and Rasmussen, R. M. 1992 Hail growth hysteresis. *J. Atmos. Sci.*, **49**, 2525–2532

Kessinger, C. J., Brandes, E. A. and Smith, J. W. 1995 'A comparison of the NEXRAD and NSSL hail detection algorithms'. Pp. 603–605 in Proceedings of the 27th conference on radar meteorology, Vail, Colorado. American Meteorological Society, Boston, USA

Knight, N. C. 1986 Hailstone shape factor and its relation to radar interpretation of hail. *J. Clim. Appl. Meteorol.*, **25**, 1956–1958

Knight, C. A. and Kight, N. C. 1970 The falling behaviour of hailstones. *J. Atmos. Sci.*, **27**, 672–681

Kry, P. R. and List, R. 1974 Aerodynamic torques on rotating oblate spheroid. *Phys. Fluids*, **17**, 1807–1892

Lemon, L. R. 1995 'Recognition of the radar 'Three Body Scatter Spike' as a large hail detector'. Pp. 533–535 in Proceedings of the 27th conference on radar meteorology, Vail, Colorado. American Meteorological Society, Boston, USA

Liebe, H. J., Manabe, T and Hufford, G. A. 1989 Millimeter-wave attenuation and delay rate due to clouds/fog conditions. *IEEE AP*, **37**, 1617–1623

List, R. 1959 Zur aerodynamic von hagelkörnen. *Z. Angew. Math. Phys.*, **10,** 143–159

1985 *Thunderstorm Morphology and Dynamics*, Second Edition. Ed. E. Kessler, University of Oklahoma Press, USA

Mason, B. J. 1971 *The Physics of Clouds.* Clarendon Press, Oxford, UK

McCormick, G. C., Allan, L. E. and Hendry, A. 1979 The backscatter matrix of ice samples: its relation to the identification of hail by radar. *J. Appl. Meteorol.*, **18,** 77–84

O'Brien, S. G. and Geodecke, G. H. 1988 Scattering of millimetre waves by snow crystals and equivalent homogeneous symmetric particles. *Appl. Opt.*, **27,** 2439–2444

Ryzhkov, A. V. and Zrnić, D. 1994 Precipitation observed in Oklahoma mesoscale convective systems with a polarimetric radar. *J. Appl. Meteorol.*, **33,** 455–464

Sachidananda, M. and Zrnić, D. 1987 Rain rate estimates from differential polarisation measurements. *J. Atmos. Oceanic Technol.*, **4,** 588–598

Seliga, T. A. and Bringi, V. N. 1976 Potential use of radar differential reflectivity measurements at orthogonal polarisations for measuring precipitation. *J. Appl. Meteorol.*, **15,** 69–76

Thwaites, S., Carras, J. N. and Macklin, W. C. 1977 The aerodynamics of oblate hailstones. *Q. J. R. Meteorol. Soc.*, **103,** 803–808

Waldvogel, A. 1974 The No jump of raindrop spectra. *J. Atmos. Sci.*, **31,** 1067–1078

Waldvogel, A., Federer, B. and Grimm, P. 1979 Criteria for the detection of hail cells. *J. Appl. Meteorol.*, **18,** 1521–1525

Waterman, P. C. 1965 Matrix formulation of electromagnetic scattering. *Proc. IEEE*, **53,** 805–812

Zrnić, D. S. 1987 Three-body scattering produces precipitation signature of special diagnostic value. *Radio. Sci.*, **22,** 76–86

Zrnić, D. S., Bringi, V. N., Balakrishnan, N., Aydin, K., Chandrasekar, V. and Hubbert, J. 1993 Polarimetric measurements in a severe hailstorm. *Mon. Weather Rev.*, **121**(8), 2223–2238